www.czasopisma.pan.pl PAN POLSKA AKADEMIA NAUK www.journals.pan.pl

Arch. Min. Sci. **64** (2019), 1, 79-92

Electronic version (in color) of this paper is available: http://mining.archives.pl

DOI 10.24425/ams.2019.126273

JANUSZ JURASZEK*#

RESIDUAL MAGNETIC FIELD FOR IDENTIFICATION OF DAMAGE IN STEEL WIRE ROPE

IDENTYFIKACJA USZKODZEŃ LIN STALOWYCH ZA POMOCĄ REZYDUALNEGO POLA MAGNETYCZNEGO

The paper presents the implementation of the method of own residual magnetic field to identify damages occurring in a steel rope. A special measuring head with 4 residual magnetic field sensors, spaced evenly every 90 degrees, was used. The measuring head was also equipped with a path or a time sensor. The measurement consists in recording normal and tangential components of the residual magnetic field and their gradients. This method has a number of advantages with regard to classic magnetic methods. It does not require special magnetisation of the rope or its special preparation for testing. Validation of the obtained test results of this rope was conducted by the classic MTR method and a very good compliance in the detection of damage was demonstrated. It was found that the strong magnetisation used in the MTR method does not affect the detection of damage to the rope using the residual magnetic field method.

Keywords: magnetic tests of steel ropes, damage to rope wires, residual magnetic field

W pracy przedstawiono implementację metody własnego magnetycznego pola rozproszenia do identyfikacji uszkodzeń występujących w linie stalowej. Zastosowano specjalną głowicę pomiarową zawierająca 4 sensory WRPM rozmieszczone równomiernie co 90. Głowica pomiarowa wyposażona była również w sensor drogi lub czasu. Pomiar polega na rejestracji składowej normalnej i stycznej WRPM i ich gradientów. Metoda ta posiada szereg zalet w odniesieniu do klasycznych metod magnetycznych. Nie wymaga specjalnego magnesowania liny oraz jej specjalnego przygotowania do badań. Przeprowadzono walidację otrzymanych wyników badań tej liny za pomocą klasycznej metody MTR i wykazano bardzo dobrą zgodność w wykrywaniu uszkodzeń. Stwierdzono, że silne magnesowanie stosowane w metodzie MTR nie wpływa na wykrywalność uszkodzeń w linie za pomocą metody WRPM.

Słowa kluczowe: badania magnetyczne lin stalowych, uszkodzenia drutów liny, metoda WRPM

* FACULTY OF MATERIALS, CIVIL AND ENVIROMENTAL ENGINERING, AKADEMIA TECHNICZNO-HUMANISTYCZNA W BIELSKU-BIAŁEJ, 2 WILLOWA STR., 43-309, BIELSKO-BIAŁA, POLAND

Corresponding author: janusz.juraszek@o2.pl

1. Introduction

In research practice, there are cases of not recognising or not detecting damage to steel ropes based on classic diagnostic methods. The work (Piskoty et al., 2009) contains the reasons for not detecting steel rope failures. For this purpose, four case studies of structural failures are presented, where the failed load carrying structure was based on wire ropes and the incidents occurred despite safety precautions. The second article (Peterka et al., 2014) shows the analysis of the damage to the rope in a hoist system of a drilling rig. The reason was the mixing of wires with different strength parameters, not to be detected with the classic magnetic methods. In this respect, it is essential to search for new methods to detect damage in the ropes. The RMF method can bring new possibilities to identify rope damage. During a very short operation of a steel rope in a hoist system of a drilling rig, the rope was significantly damaged. The wires of the upper layer of the cable strands were damaged. This damage was not caused by fatigue of the material; the analysis of the mechanical test results of the new rope revealed the fact that the rope was manufactured in another rope grade – different from the class declared by the manufacturer. It was also found that the wires of the top layer reporting damage were made of wires of different rope grades. Mixing wires of low and high strength in the upper layer of the rope strand caused different straining of wires in the specific (given) layer; thus, wires having lower strength begun to release from the strands and deform, which led to the development of fractures at the weakened places.

There are a number of publications in the literature regarding the analysis of damage occurring in flat specimens identified by the RMF method. For example, damage identification, but only in flat, tensioned 12mm thick specimens, was analysed in the work (Shui et al., 2015). The places where the normal component Hn is zero indicated damages to the specimen.

The RMF method also allows the identification of stress concentration zones. An article (Shuchun et al., 2015) discussing the dependence of the occurrence of stress concentration zones in the 3 and 4-point bending test on the distribution of Hp and Hn components, as well as the reduced stress according to the Huber-Misses-Hencky hypothesis, is an interesting work on this subject.

The residual magnetic field method is used in the diagnostics of ferromagnetic structural elements. It allows for the location of cracks, microcracks, closed cracks, which are difficult to locate by traditional methods. Knowing the previous magnetic image of the examined element, it is possible to detect places of stress concentration before the occurrence of cracks or microcracks. This is one of the few methods that "a priori" indicates dangerous places in the structure (Hailong et al., 2017). To promote study in this area, the magnetic gradient tensor (MGT) of the self-magnetic leakage field (SMLF) on the fracture zone of crack and stress concentration was measured using a 2 or 3-axis magnetometer. The magnetomechanical model supplemented by FEM analyses is presented in the work (Pengpeng et al., 2017)

The underlying mechanism behind MMM has been explained in the literature, but the sensitivity to stress concentration has not been satisfactorily investigated. In the paper (Zhichao et al.,2017), both the normal and tangential components of the stress-induced MMM signal were measured by permanently installed magnetic sensor arrays on specimens made from three grades of L80 alloy steel and 20 other structural steels. A theoretical study on the method of metal magnetic memory was included in the works (Wang et al., 2010; Bulte et al., 2002). A hypothesis of how stress or the stress state affects selected ferromagnetic material properties was presented.

A theory was introduced at the atomic level of the cause of the magnetomechanical effect in which the spin-spin compression with magnetic moments affects the change in the magnetocrystalline anisotropy. Changes in the magnetic domain wall settings under mechanical stress load were explained (Bulte et al., 2002). Practical work to implement the RMF method for structural steels was presented in the work (Xionga et al., 2016) and the interesting use of magnetic field sensors located permanently in the work (Li et al., 2017).

The work on the influence of temperature and stress on the level of residual magnetic signal for structural steel Q 345B is also interesting (Huang et al., 2017). The researchers determined the tangential and normal components of the residual magnetic field for different temperatures in the range of 25-250°C and different normal stress values. They also presented research on the microstructure and cracks caused by the temperature gradient. Similar studies were conducted by Leng J.C. and others (Leng et al., 2013) in the field of plastic deformation of low carbon steel (they investigated the effect of plastic deformation on magnetic behaviour).

The study of the impact of mechanical processing on the level of own stresses and the associated level of RMF components was analysed by Wilson J.W. (Wilson et al., 2007). Flat specimens were loaded in special holders. He suggested calibration using an x-ray diffraction method, which enables a precise determination of deformations in individual crystallographic planes and then the own strains.

It allows to take proper preventive actions with an appropriate advance (Yao et al., 2012; Ren et al., 2001; Dong et al., 2005). In the last century this method, initially the issue of boiler tubes, was studied by Dubov. He led to putting the naming in order and implementation of standards for the method, defined by him as the metal magnetic memory method. A significant contribution to the research of steel ropes was introduced by Prof. J. Hankus (Hankus, 2000; Hankus, 2002). He was also using the RMF method to evaluate fatigue wear of steel ropes (Hankus et al., 2006).

Juraszek J. applied the RMF method to study the residual stress assessment in crimp connectors. In the mining industry, he applied FBG optical fibres to analyse deformations and loads of steel ropes and brake rod of the hoist machine (Juraszek, 2019 a,b). FBG fibre optic measurements can comprise validation of the places designated by the RMF method. Further works conducted jointly by Grzywa A (doctoral thesis) concerned the implementation of the residual magnetic field method to a number of machine parts and components, including fatigue tests of welded joints used in the construction of pressure vessels, power joints in combination with FEM analysis, pitting process tests. Many years of research also concerned crane beams, drive shafts for mechanical presses, support structures for high-voltage pylons. In the paper (Kosoń-Schab et al., 2016), the problem of continuous inspection of crane's frame using the metal magnetic memory method is considered. The influence of operational variations on the self-magnetic flux leakage signal is investigated and quantitatively analysed based on the experimental results obtained on a laboratory scaled overhead travelling crane. Numerical magnetic flux analysis conducted with the use of the FEM ANSYS program is presented in the work (Zhang et al., 2018). Basic concepts regarding the subject of control, control measures, pre-test procedures, control procedures as well as safety requirements for the RMF method are included in the reference standards (ISO, 2007). The analysis of the PN-ISO 24497-2:2009 standard, which contains the basic concepts regarding the subject of control, control measures, pre-test procedures, control procedures as well as safety requirements for the RMF method.

2. Theoretical background

In the method of Metal Magnetic Memory, the distribution, determined near the surface of the tested element, of the vertical component of the intensity of the residual magnetic field H_p is used to assess the degree of material strain. Analysing the general case inside the ferromagnetic element with permeability μ , induction is produced $B = \mu H$ where H is the intensity of the magnetising field, in the case of the RMF method, this is the Earth's magnetic field. The creation of the residual magnetic field over the surface of the element is caused by an induction component perpendicular to the surface of the tested element B_p. If there is an area with different magnetic permeability in the magnetic induction flux path inside the element, there is a tangential component B_τ created. The value of the vertical component of the intensity of the residual magnetic field H_p is directly proportional to the vertical value of the induction component B_p:

$$H_p = \frac{1}{\mu_o} B_p \tag{1}$$

constant μ_o in the formula means air magnetic permeability and is equal

$$\mu_o = 2\pi \cdot 10^{-7} \frac{V \cdot s}{A \cdot m}$$

Vertical component increase ΔH_p is also directly proportional to the increase ΔB_p:

$$\Delta H_p = \frac{1}{\mu_o} \Delta B_p \tag{2}$$

Value B_p is proportional to the induction gradient B along the tested element:

$$B_p \sim \frac{\Delta B}{\Delta z} \tag{3}$$

the same value H_p is also proportional to the gradient B along the tested object:

$$H_p \sim \frac{l}{\mu_o} \frac{\Delta B}{\Delta z} \tag{4}$$

The induction decreases when the induction flux enters an area with lower permeability. In such a situation, the induction vertical component and the vertical component of the residual field have a positive sign. In contrast, the induction increases when the induction flux leaves the area with lower permeability. The induction vertical component and the vertical component of the residual field have a negative sign. Above the centre of this area, the value H_p reaches zero. In areas with the same magnetic properties, the induction lines run parallel to the surface and there is no residual magnetic field over the material surface.

A change in induction ΔB in the section Δz caused by stress can be calculated as:

$$\Delta B = \lambda_{H,T} \cdot \Delta\sigma, \lambda_{H,T} = \left(\frac{\Delta B}{\Delta \sigma} \right)_{H,T} \tag{5}$$

The expression $\lambda_{H,T}$ means the sensitivity of the material magnetoelastic phenomenon at the constant magnetising field H and at the constant temperature T. Taking these dependences into account, we obtain:

$$H_p \sim \frac{l}{\mu_o} \lambda_{H,T} \cdot \Delta\sigma \tag{6}$$

component value H_p is directly proportional to the change in intensity in the section Δz and depends on the sensitivity of the magnetoelastic phenomenon of the tested object.

The relation between the vertical component of the field strength and components of the stress state depends on a lot of factors, in addition to the magnetising field strength and temperature, also on the type of deformation (tension, compression, complex states, mechanical load of the tested element).

3. Research object

The object of the research was a rope with the structure Seale 6x19+NF with a diameter of 16 mm. The rope is made of 6 rope strands with 19 wires in two layers: in the first layer 9 wires, in the second one 9 wires with a larger diameter. Inside the rope, there is a core made of natural fibres.

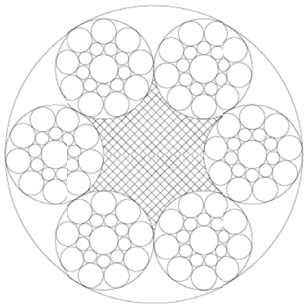

Fig. 1. Cross section of Seale 6X19+NF rope

The basic parameters of the rope 16 S 6X19+NF in accordance with the PN-70/M-80222 standard. The researchers used a metal magnetic memory tester equipped with a device recording stress concentrations TSC-3M-12. It is equipped with a special measuring head for testing steel ropes consisting of four Hall-effect sensors spaced evenly every 90 degrees on the head perimeter. It has a replaceable sleeve that is selected for the diameter of the object (rope) tested in the range from 12 to 60 mm. In addition, the head is equipped with a path sensor that starts the measurement every 0.5mm as well as a time sensor (timer) that starts the measurement, for example, every 0.2 sec.

The recording device consists of:

– multi-channel recorder (12 channels) allowing the use of various types of measuring heads,

– memory cards that allow to record measurement results for about 1-15 days without the need to transfer data to a computer. The basic measuring range of the TSC device for the component of the residual magnetic field H_p for each of the 12 channels is ±2000 A/m. An unquestionable advantage of this device is its low weight of 0.6 kg. A classic magnetic measuring head weighs 60 kg.

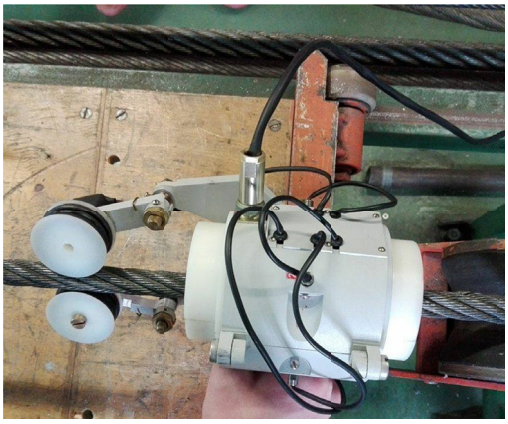

Fig. 2. Measuring head for testing ropes

The accuracy of the measurements is influenced by the size of the gap between the rope and the tops of the Hall-effect sensors. We should strive to make the gap as small as possible and the same for all 4 sensors. In practical measurements, the size of the gap is a compromise between unevenness of the rope diameter and the previously mentioned gap minimisation. In practice, this gap is about 1mm. The tests were conducted in laboratory conditions under specified thermal and environmental conditions and constant magnetic conditions (no external disturbances to the magnetic field). The impact of these factors on the accuracy of the tests can be considered as irrelevant.

Description of damages in the rope

The main essence of the experiment was the introduction of various types of damages in precisely defined places along the length of the tested rope. In the next stage, the rope was mounted on a test stand consisting of two pulleys. Earlier, the rope ends were braided at the length L. The tested rope is a loop that moves around driven by a wheel. The purpose of the test was to identify damages introduced into the rope by the RMF method and to validate the tests by a classic rope test method requiring strong magnetisation. The view was also verified that earlier tests using strong magnetisation would prevent the test by a method using its own residual magnetic field. To this end, the sequences of the course of the experiment were determined as follows:

1) The first phase covered tests that did not require strong artificial magnetisation, i.e. using the RFM method,
2) In the second one, classic tests by the MTR method were conducted,
3) The last one covered another test by the RMF method.

The following damages were introduced in the rope at places defined by the distance from the starting point:

- rope strand in the core – 2 damages at the length of 0.5 m,
- splice – 7 damages at the length of 5.9 m,
- metal ball in the core with a diameter of 3 mm,
- two wires cracked in 12 places at the length of 2.35 m,
- four wires cracked in 6 places at the length of 2.45 m,
- six wires cracked in 4 places at the length of 2.40 m.

The test of the normal and tangential components of the residual magnetic field around the rope was conducted with the use of 4 sensors shown in Fig. 3 as S1-S4. The sensors marked with odd numbers S1 and S3 were placed horizontally in relation to the rope, while the even sensors S2 and S4 were placed vertically. The measuring head was constructed in such a way that it was able to rotate 45 and 22.5 degrees in relation to the rope axis. Each sensor measured two components, tangential and normal.

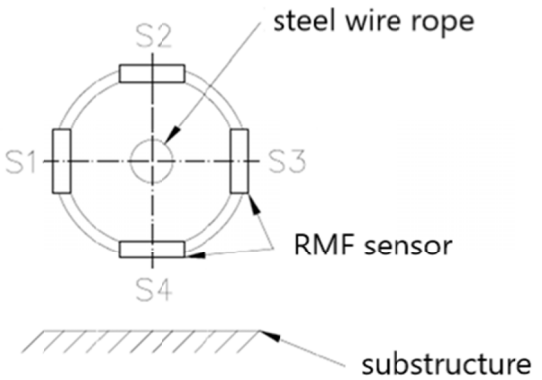

Fig. 3. Diagram of the location of the sensors in the measuring head

During the measurement, 8 components of the residual magnetic field were recorded:

- Hp_1, Hp_3, Hp_5, Hp_7 – tangential components,
- Hp_2, Hp_4, Hp_6, Hp_8 – normal components.

During the test, the head is fixed on a special tripod while the rope moves.

4. Rope magnetic test results

As a result of the measurements conducted, distributions of individual components of the residual magnetic field were obtained. The rope does not have to be specially prepared for the test. Distribution of the RMF tangential component recorded for the sensor S1 is shown in Fig. 4. This probe recorded precisely all 32 damages in the tested rope. In the graph, they are in the form of clear impulse changes in the tangential component value. The image of two wires cracked in 12 places in the middle part of the rope is in the range of 12,500-15,000 mm in the form of 12 im-

pulses in the middle part of the figure. In the final part of the graph, there are 4 "peaks" with values of –170 to –230 A/m corresponding to 6 wires cracked in 4 places. The next 6 "peaks" unequivocally identify 6 wire cracks at the length of 2,400 mm. The impulse for the x-coordinate value approx. 10000 mm from the value of –200 to 230 A/m is a magnetic image of a steel ball placed in the rope core with a diameter of 3 mm. The remaining 7 impulses at the length of 5,800 mm to 8,750 mm reflect the effect of the rope splice on the tangential component distribution, the values of which are in the range –600 to 100 A/m. The initial part of the graph concerns 2 damages located in the rope core. It should be emphasised that all the damages introduced into the rope have been precisely located and exactly coincide with the damages in the tested rope.

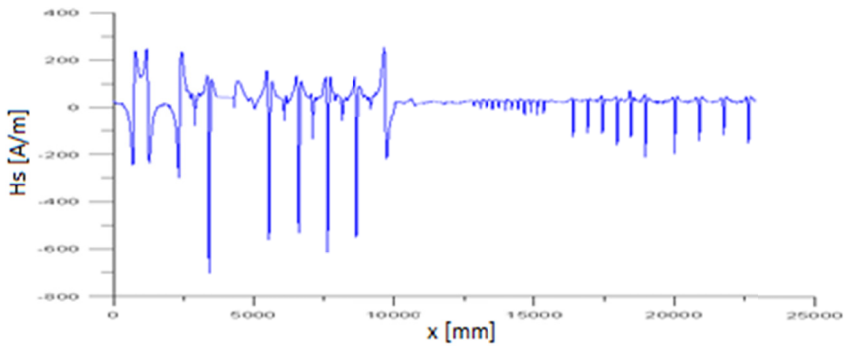

Fig. 4. Distribution of the tangential component along the tested rope

Then, tests on the rotation of the measuring head by 45 and 22.5 degrees in relation to the vertical axis of the rope were conducted. The results of measurements of the tangential component distribution from the S1 sensor for the case of rotation by 45 are shown in Fig. 5. It can be observed that the upper recorded values of the tangential component have grown from 230 to approx. 400 A/m. Signals induced by individual damage groups are stronger. Identification of individual damages is as precise as for the 0-degree position.

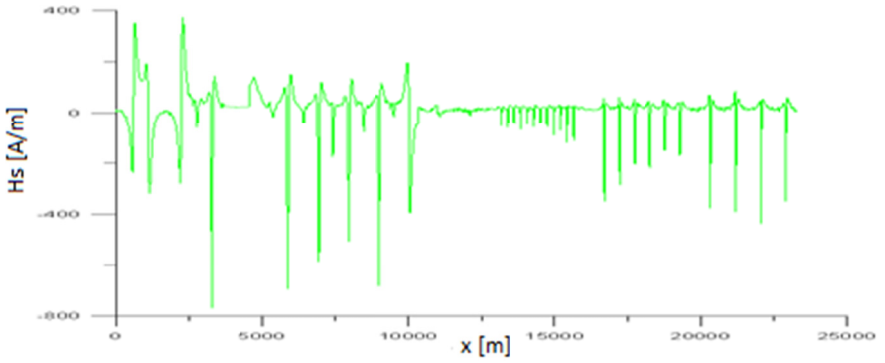

Fig. 5. Distribution of the tangential component along the tested rope for the case of rotation of the measuring head by 45°

Rotation by further 22.5° did not significantly change the magnetic image of the tested rope (Fig. 6).

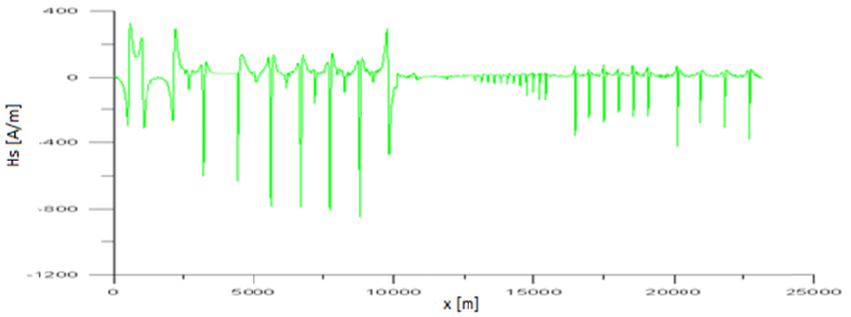

Fig. 6. Distribution of the tangential component along the tested rope for the case of rotation of the measuring head by 22.5°

The distribution of the normal component recorded with the S1 sensor is shown in Fig. 7. It can be noticed that 32 damages introduced into the rope cause a similar distribution of the normal component as in the previous graphs showing the distribution of the tangential component. The tangential component allows precise location of damages in the rope. It can be observed that the values of the normal component in relation to the tangential component are much higher. They are in the range of 2700 A/m to –2500 A/m. These are values exceeding the measuring range of the device. This is due to the repeatedly conducted test by a classic magnetic method that requires strong magnetisation of the rope to identify magnetic field disturbances. This indicates that multiple early magnetisations of the rope does not limit the identification of damages in the rope by the RMF method, on the contrary, it strengthens the magnetic image.

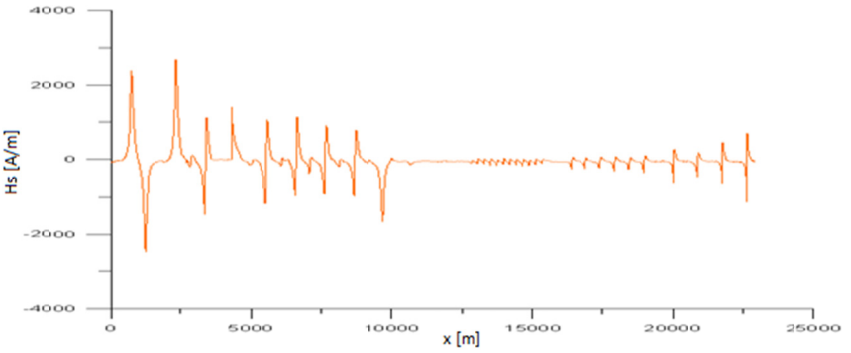

Fig. 7. Distribution of the normal component along the length of the rope

In the assessment of the damages to the rope, in addition to the analysis of distributions of the normal component, in particular, in places where the value of the component $Hn = 0$ (microcrack, crack, discontinuity), analyses of tangential component distributions, where places of local

extremes determine damage locations in the rope, gradient analysis of both residual magnetic field components is also performed. K_{in} coefficient determining the intensity of the perpendicular and/or tangential magnetic field gradient is used to quantify the level of stress concentration. This coefficient is determined by the formula:

$$K_{in} = \frac{\left|\Delta H_p\right|}{l_k}, \left[\frac{\mathrm{A}}{\mathrm{m}^2}\right] \tag{7}$$

where: ΔH_p is the difference of H_p fields between two neighbouring scanning points; l_k is the distance between these neighbouring points.

The highest value of the tangential and normal gradient of the own residual magnetic field indicates the zone of maximum stress concentration. On the basis of the number of previous laboratory tests, for ferromagnetic machine parts, it has been determined that dangerous places occur at values above 10 A/m/mm. In the case of steel ropes, it results from the tests that the value of the K_{in} coefficient should be limited to 5 A/m/mm. The distribution of the tangential component gradient along the length of the rope is shown in Fig. 8.

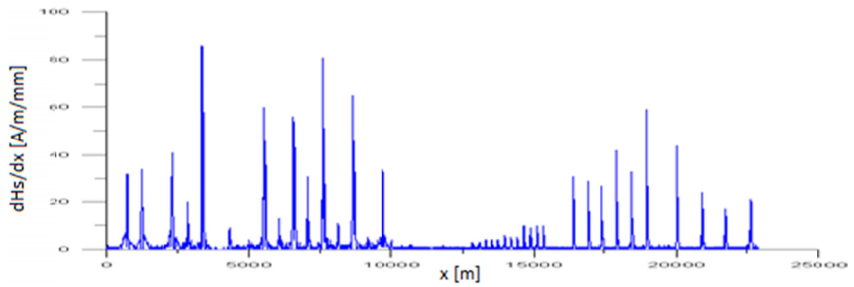

Fig. 8. Distribution of the tangential component gradient along the length of the rope

The gradient values vary from 0 to 87 A/m/mm. Assuming the threshold value of 5 A/m/mm enables identification of all damages introduced into the rope. Similarly, the distribution of the normal component gradient can be determined. Due to the higher values of the normal component, the gradient values of this component are in the range of 0-240 A/m/mm. The distribution is similar to the tangential component.

Analysing individual damages in the rope, it can be stated that, for example, for the damage No. 4, the sensors of the normal component Hn2, Hn4 are characterised by the highest sensitivity, while for the tangential component the sensors Hs5 and Hs7 Fig. 9. It can be noticed that where the normal component Hn2 is zero, the tangential component Hs1 reaches an extreme of 1900 A/m/mm. This is reflected in the graph of gradients of the tangential and normal components Fig.10. The highest values are achieved by the component gradients Hp1 and Hn2.

The magnetic image obtained by means of the classic magnetic method is shown in Fig. 11. It can be noticed that both methods precisely locate the damage in the rope, for example, the damage No. 4. The RMF method gives a signal earlier in relation to the information obtained from the classic magnetic method.

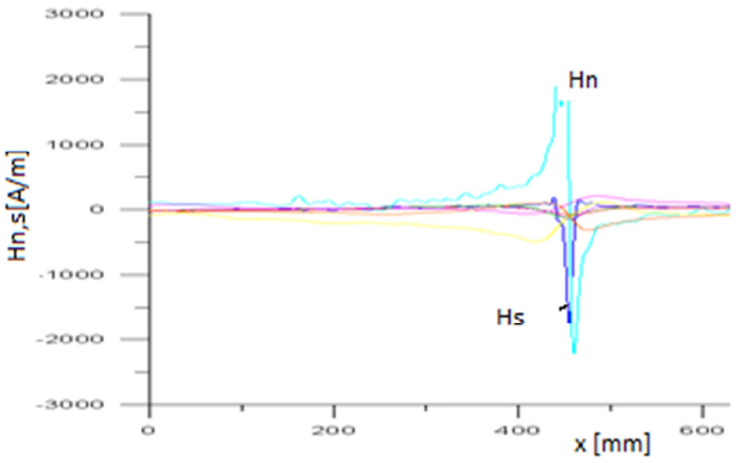

Fig. 9. Distribution of normal and tangential components for the damage No. 4

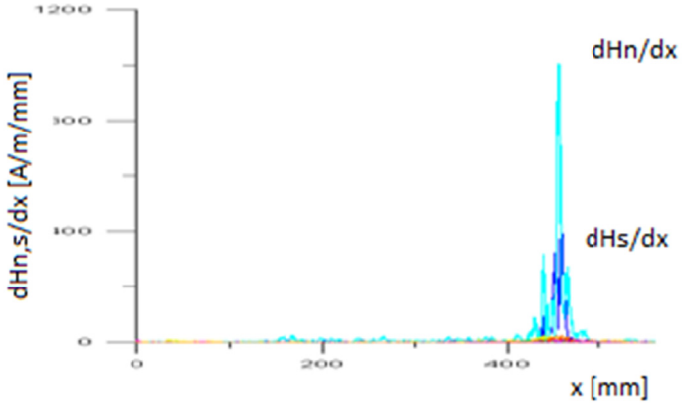

Fig. 10. Distribution of normal and tangential component gradients for the damage No. 4

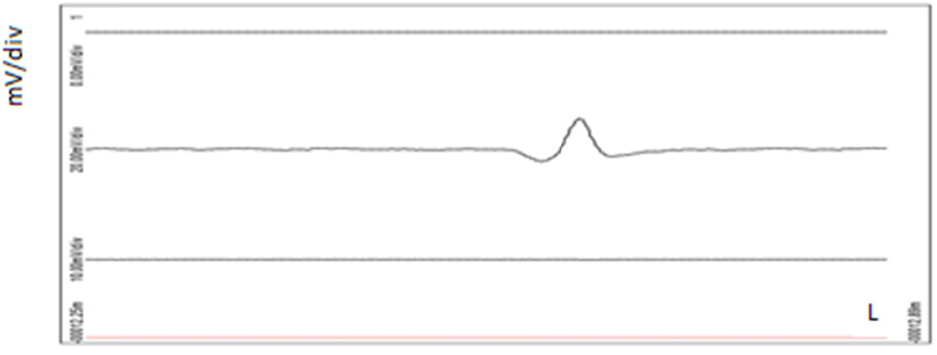

Fig. 11. Image of the damage No. 4 by the classic magnetic method

5. Industrial research

The test covered a hoisting rope of a mountain cable car with the following parameters:
- construction: SF + 6(1 + 7 + 7 + 7 + 14), load carrying cross section: F_n = 588 [mm^2]
- rope diameter: 38 [mm].

The classic magnetic method with strong magnetisation and the RMF method were applied. The test results of the splice area by the RMF method are shown in Fig. 13. The highest values of the normal component can be observed at the beginning and at the end of the splice. The Hn values reach 1800A/mm. Higher values also mean larger strain in the rope wires in this area. In the remaining part of the rope, the values of the normal component are in the range of –500 to 500 A/mm.

When comparing the results obtained by the RMF method with the results using the classic magnetic method, it can be concluded that both methods are equally as precise at identifying the rope splice. They indicate characteristic peaks in the same places, Fig. 12-13. The RMF method also indicates a larger strain or level of reduced stress in the starting and end coils of the splice.

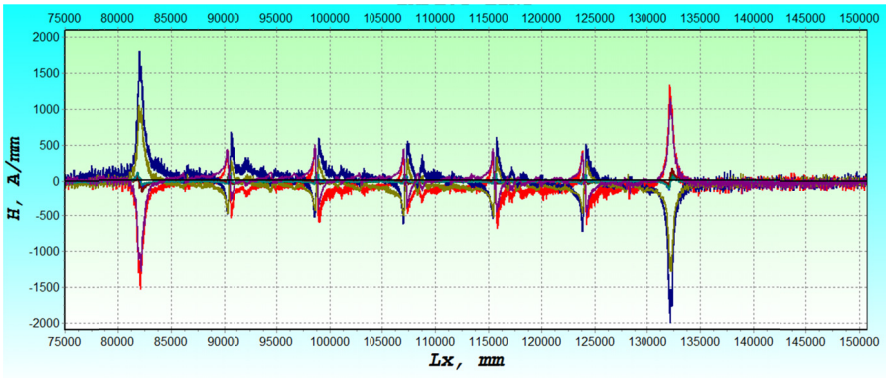

Fig. 12. Distribution of RMF component values in the rope splice

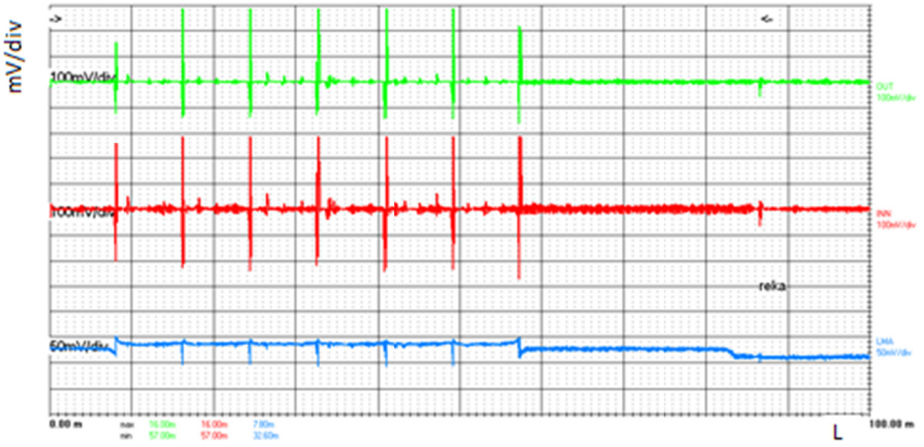

Fig. 13. Magnetic image of the rope splice by the classic magnetic method

An important advantage of the RMF method, especially during field studies, is a much lighter measuring head (about 40 times), no magnetisation required, and preparation of the rope surface. This makes the RMF method less time-consuming and, which is important, less cost-intensive at the same time. At the present stage of the development of rope tests by the RMF method, one can speak about its qualitative image. Conducting further intensive research from the beginning of the rope operation, consisting in recording its magnetic image related to the degree of rope strain and creating an appropriate database of magnetic images can give a quantitative image of RMF tests in the future. It is, therefore, necessary to create databases of magnetic images of individual types of ropes depending on the load and operation time. The process of creating these bases can be accelerated by laboratory tests, where a given type of rope will be loaded with a real fatigue load spectrum combined with simultaneous monitoring of the magnetic image of the tested rope.

6. Conclusions

The use of the Metal Magnetic Memory method (Residual Magnetic Field) enabled the diagnostics of the technical state of the tested rope. The tests clearly showed 32 damages introduced earlier into the rope, which were also identified by the classic magnetic MTR method.

The MPM method has a number of important advantages in relation to the classic MTR method, which can include:

- no need for artificial magnetising of the tested object,
- no need to clean the tested element,
- less complicated measuring equipment,
- ease of testing,
- owing to different types of measuring heads it is possible to test various types of elements made of ferromagnetic materials,
- a significantly lower weight of the MPM test head (1.5 kg) than the head used in the MTR test (60 kg).

The RMF method offered in the work to identify damages in a rope is an interesting addition to the classic magnetic methods used. It allows a precise identification of damages in the rope and location of the splice. The special head presented in the work, with 4 sensors spaced evenly every 90 degrees, has been proved useful in both laboratory and industrial tests. The entire head can be rotated by any angle in relation to the global reference system. The head is universal because it is possible to conduct tests of ropes with different diameters. With the RMF method, it is possible to detect places of material defects or stress concentration zones already at the stage of their formation, which is very important in order to detect damage at an early stage of its development. It is also of great importance that the time of diagnostic tests is short, which translates into the low cost of such tests. The conducted laboratory and field experiments confirmed the possibility of early detection of damages in a rope by the RMF method.

References

Bulte D., Langman R., 2002. *Origins of the magnetomechanical effect*. Journal of Magnetism and Magnetic Materials **251**, 229-243.

Dong L.H., Xu B.S., Dong S.Y., Chen Q.Z., Wang Y.Y., Zhang L., 2005. *Metal Magnetic memory testing for early damage assessment in ferromagnetic materials*. J. Cent. South. Univ. Technol. **12** (S2), 102-106.

Er-gang Xionga, Na-na Zhao, Zhao-qi Yan, Lan-wei Yang, Han He, 2016. *Magnetic Nondestructive Testing Techniques of Constructional Steel*. MATEC Web of Conferences MATEC **43**, 03002.

Hailong Chen, Changlong Wang, Xianzhang Zuo., 2017. *Research on methods of defect classification based on metal magnetic memory*. NDT & E International **92**, 82-87.

Hankus J., 2000. *Budowa i własności mechaniczne lin stalowych*. Katowice, Główny Instytut Górnictwa.

Hankus J., 2002. *Zintegrowane metody badań i oceny stanu bezpieczeństwa lin stalowych*. Prace Naukowe GIG, Górnictwo i Środowisko **4**.

Hankus J., Hankus Ł., 2005. *Niekonwencjonalne metody badań diagnostycznych drutów lin stalowych*. Wiadomości Hutnicze **2**.

Hankus J., Hankus Ł., 2006. *Nowa metoda badań diagnostycznych lin stalowych z wykorzystaniem magnetycznej pamięci metalu*. Prace Naukowe GIG, Górnictwo i Środowisko nr 2.

Huang H., Quian Z., 2017. *Effect of Temperature and Stress on Residual Magnetic Signals in Ferromagnetic Structural Steel*. IEEE Transactions on Magnetics **53**, 1.

ISO 24497-1:2007 Non-destructive testing – metal magnetic memory – Part 1: vocabulary.

ISO 24497-1:2007 Non-destructive testing – metal magnetic memory – Part 2: general requirement.

Juraszek J., 2019a. *RMF Non-destructive Testing of Gantry Crane Materials (ISSN 1996-1944) Special Issue "Non-destructive Testing of Materials in Civil Engineering*. Materials **12** (4), 564.

Juraszek J., 2019b. *Światłowodowa i optyczna analiza odkształceń*. Wydawnictwo Naukowe ATH Bielsko-Biała.

Kosoń-Schab A., Smoczek J., Szpytko J., 2016. *Crane Frame Inspection Using Metal Magnetic Memory Method*. Journal of KONES Powertrain and Transport **23**, 2.

Leng J.C., Liu Y., Zhou G.Q., Gao Y.T., 2013. *Metal Magnetic Memory Signal Response to Plastic Deformation of Low Carbon Steel*. NDT E Int. **55**, 42-46.

Pengpeng Shia, Ke Jinb, Xiaojing Zhenga, 2017. *A magnetomechanical model for the magnetic memory method*. International Journal of Mechanical Sciences 124-125, 229-241.

Peterka P., Krešák J., Kropuch St., Fedorko G., Molnar V., Vojtko M., 2014. *Failure analysis of hoisting steel wire rope*. Engineering Failure Analysis **45**, 96-105.

Piskoty G., Zgraggen M., Weisse B., Affolter Ch., Terrasi G., 2009. *Structural failures of rope-based systems*. Engineering Failure Analysis **16**, 1929-1939.

Ren J.L., Song K., Wu G.H., Lin J.M., 2001. *Mechanism study of metal magnetic memory testing*. Procedings of the 10th Asia-Pcyfic Conference on Non-Destructive Testing Birsbane Australia, 17-21.09.2001.

Shuchun Yi, Wei Wang, Sanqing Su., 2015. *Bending experimental study on metal magnetic memory signal based on von Mises yield criterion*. International Journal of Applied Electromagnetics and Mechanics **49**, 547-556.

Shui G., Li. Ch., Yao K., 2015. *Non-destructive evaluation of the damage of ferromagnetic steel using metal magnetic memory and nonlinear ultrasonic method*. International Journal of Applied Electromagnetics and Mechanics **47**, 1023-1038.

Stevens K.J., 2000. Nondestr. Test. Eval. Int. **33**, 111.

Wang Z.D., Yao K., Deng B., Ding K.Q., 2010. *Theoretical studies of metal magnetic memory technique on magnetic flux leakage signals*. NDT & E International **43**, 4, 354-359.

Wilson J.W., Tian G.Y., Barrans S., 2007. *Residual magnetic field sensing for stress measurement*. Sensors and Actuators A **135**, 381-387.

Yao K., Wang Z.D., Shen K., 2012. Experimental Research on Metal Magnetic Memory Method Experimental Mechnics **52**, 305-314.

Zhang O., Wei X., Yan S., 2018. *Numerical Analysis of Magnetic Flux Leakage of Transverse Defects of Sucker Rod*. Journal of Testing and Evaluation.

Zhichao Li, Steve Dixon, Peter Cawley, Rollo Jarvis, Peter B. Nagy, Sandra Cabeza, 2017. *Experimental studies of the magneto-mechanical memory (MMM) technique using permanently installed magnetic sensor arrays*. NDT & E International **92**, 136-148.